http://www.oceanpress.com.cn
E-mail: hyxb@263.net

In-line response of vertical cylinders in regular and random waves

LI Yok-sheung, SU Wei, ZHAN Jiemin*, ZHAN Sheng

1. Department of Civil & Structural Engineering, The Hong Kong Polytechnic University, Hong Kong, China
2. Department of Applied Mechanics and Engineering, Zhongshan University, Guangzhou 510275, China

Received 20 June 2006; accepted 22 December 2006

Abstract

The in-line response of a vertical flexibly mounted cylinder in regular and random waves is reported. Both theoretical analyses and experimental measurements have been performed. The theoretical predictions are based on the Morison equation which is solved by the incremental harmonic balance method. Experiments are then performed in a wave flume to determine the accuracy of the Morison equation in predicting the in-line response of the cylinder in regular and random waves. The interaction between waves and vibrating cylinders are investigated.

Key words: in-line response; cylinder; waves; IHB method

1 Introduction

Many cost-effective offshore structures have been fabricated for oil and gas exploration and production. One example of such offshore structures is the tension leg platform, which is usually supported by concrete piles as the foundation or tension legs as the anchoring device. Another common type of platforms is the spar platform, which can be considered as a floating vertical cylinder, stabilized by mooring lines connected to the seafloor. Besides oil production, floating fish cages are often used by the aquaculture industry to rear fish due to the rapid decline of fish stocks in the open oceans.

Wave forces are the major component of the total forces experienced by offshore structures. Usually the amplitude of the motion of the structure induced by the incident wave is assumed to be small. The incident wave is first considered to be scattered by a fixed structure. Then the platform structure is considered to be forced into motion by the incident and scattered waves. The forced oscillation of the structure in turn generates outgoing waves.

A wide variety of previous investigations have studied the loading of stationary cylinders in unidirectional oscillatory waves. Sarpkaya and Isaacson (1981) reviewed early studies over a range of Keulegan—Carpenter number. Tatsuno and Bearman (1990) investigated the vortex patterns that can arise in different ranges of KC, and in certain cases, their relationship with the cylinder loading. Qiu and Zhu (1986, 1985) studied the diffraction problem of two piers with unequal diameters, and gave formulas for calculating wave forces on the basis of MacCamy—Fuchs linear wave diffraction theory. Miu and Liu (1991) used a type of local disturbance source which distributed on the sectional contour of the cylinders together with the well-known source to estimate the three-dimensional hydrodynamic forces on

* Corresponding author. E-mail: stszjm@mail.sysu.edu.cn

single cylinder of arbitrary section.

Vibration of elastically mounted cylinders in water waves has been simulated and observed by a lot of investigators. The investigations involved three types of elastically mounted cylinders: elastic vibration only in the transverse (cross wave) direction, the in-line direction, and bidirectional vibration, which allows simultaneous motion in the transverse and in-line directions. For the transverse vibration, the resonant response has been investigated by Angrilli and Cossalter (1982), Kaye and Maull (1993) and Hayashi and Chaplin (1998). For the in-line vibration, Williamson (1985) predicted resonant in-line vibration of a cylinder by deducing an equation of motion involving the Morison equation for flow-induced in-line forces. Li et al. (1997) carried out both theoretical analyses and experimental measurements. The theoretical predictions are based on the Morison equation which is solved by the incremental harmonic balance method. Experiments were performed in a wave flume to determine the accuracy of the Morison equation in predicting the in-line response of the cylinder in regular and random waves. For random waves, it is found that the in-line response can be predicted accurately by a superposition of the response to wave components of different frequencies using the Morison equation only when the ratio of wave height to cylinder diameter is small. For the bidirectional vibration, Sawaragi et al. (1977) treated the maximum response in the transverse and in-line directions as a function of ratio of the natural frequency to the wave one.

The importance of wave—structure interaction tests is increasing because of the occurrence of high energy waves, tsunami and underwater explosion phenomena. Murata et al. (2004) performed a series of near-field underwater explosion tests to investigate the response of model target during underwater shock and bubble pulse loading.

McIver et al. (2003) made a numerical and analytical investigation of the response of a fluid to a two-dimensional moving structure in a prescribed mode. Localizing oscillations can be found at a frequency close to that of the trapped mode, but with amplitude that decays slowly with time. On the basis of the potential theory in cylindrical coordinates with Fourier spectral elements, Chern et al. (2001) presented a numerical model of the three-dimensional hydrodynamics of an inviscid liquid with a free surface.

Sarkar and Taylor (2001) analyzed the nonlinear multi-degree-of-freedom dynamics between nonlinear waves and nonlinear moored vessels using a two-scale perturbation method developed by Sarkar and Taylor (1998). Swan et al. (1997) performed a physical model study of waves around the Brent Brave gravity based structure. They showed that the three large, closely spaced legs generated considerable wave—structure interaction. Chen (1998) presented an analysis of the emotion of a vertical cylinder using three-dimensional equations of motion under the simultaneous action of three components of ground acceleration. The dynamic response of a cylinder is approximated by the displacements in the fundamental modes of vibration. Broderick and Leonard (1995) studied the behavior of a highly deformable membrane to ocean waves by coupling a nonlinear boundary element model of the fluid domain with a nonlinear finite element model of the membrane. A large-scale test conducted by them verified the numerical prediction of the structure displacements and the changes in the wave field.

Chaplin et al. (1997) analyzed the results of two series of experiments concerned with the response of a single vertical cylinder in the inertia regime in steep non-breaking waves. They recorded first the loading on a cylinder when it was held stationary, and then its response to the same waves when it was pivoted just above the floor of the wave flume and supported at the top by springs in the horizontal plane. Peak loading on a stationary cylinder

was found to exceed the prediction of a Morison model. At low frequency ratios, there is clearly some feedback from the motion to the excitation. Peak accelerations in the steepest waves are found to be limited approximately to those that would occur if the maximum loading was applied as a step change.

The prediction of the response of a flexibly mounted circular cylinder in wavy flows is a difficult problem due to the complexity of fluid—structure interaction mechanisms.

The study of the response of a horizontal cylinder to both regular and random waves has been investigated by Li and Zhan (1997). In this paper, the study on vertical cylinders are reported. The mounting of the vertical cylinders are specially designed so that they can maintain their vertical position while vibrating in the horizontal direction. They may be used as breakwaters to attenuate incoming waves from the open sea. The theoretical predictions are based on the Morison equation which is solved by the incremental harmonic balance (IHB) method (Lau and Zhang, 1992; Lau and Cheung, 1981).

2 Theoretical considerations

The equation used to describe the in-line response of an oscillating vertical circular cylinder to waves is the Morison equation which can be written as follows, taking into account the effect of the wave-induced orbital motions:

$$M\ddot{x}+c\dot{x}+kx=\int_{-d}^{0}C_M\frac{\rho\pi D^2}{4}\dot{u}\,dz+\int_{-d}^{0}C_d\frac{\rho D}{2}(u-\dot{x})\sqrt{(u-\dot{x})^2+w^2}\,dz \quad (1)$$

where M is the mass of cylinder plus the added mass ($=m+C_a\rho\pi D^2L/4$, m is each cylinder mass, ρ the fluid density, D the cylinder diameter, and C_a is the added mass coefficient), d the water depth, c the structural damping of cylinder system, k the effective spring stiffness, C_d the drag coefficient and C_M the inertia coefficient, x is the cylinder displacement, u the horizontal velocity component of fluid particles, and w is the vertical velocity component of fluid particles. The overdot in Eq. (1) represents differentiation with respect to time t.

The horizontal and vertical fluid velocities u and w at location z (measured upwards from the still water level) under a small amplitude wave of amplitude $H/2$, angular frequency ω, wave number k are given by

$$u=\frac{gHk}{2\omega}\frac{\cosh k(d+z)}{\cosh kd}\cos\omega t$$

$$w=-\frac{gHk}{2\omega}\frac{\sinh k(d+z)}{\cosh kd}\sin\omega t \quad (2)$$

where g is the gravitational acceleration.

Equation (1) can be written in the following form:

$$M\omega^2\ddot{x}+c\omega\dot{x}+kx+C_M\frac{\rho g\pi D^2H}{8}\tanh kd\sin\tau-\int_{-d}^{0}C_d\frac{\rho D}{2}(u-\omega\dot{x})\sqrt{(u-\omega\dot{x})^2+w^2}\,dz=0 \quad (3)$$

where differentiation now is with respect to τ instead of time, and $\tau=\omega t$.

For simplicity, Eq. (3) is rewritten in the compact form:

$$F(\ddot{x},\dot{x},x,\tau)=0. \quad (4)$$

Equation (4) is solved by the IHB (incremental harmonic balance) method. Let x_0 be an approximate solution and $x_0+\Delta x_0$ be a more accurate solution to Eq. (4). Then, using the Taylor series expansion, we have

$$F(\ddot{x}_0,\dot{x}_0,x_0,\tau)+\frac{\partial F}{\partial\ddot{x}_0}\Delta\ddot{x}_0+\frac{\partial F}{\partial\dot{x}_0}\Delta\dot{x}_0+\frac{\partial F}{\partial x_0}\Delta x_0=0 \quad (5)$$

with

$$\frac{\partial F}{\partial\ddot{x}_0}=M\omega^2,$$

$$\frac{\partial F}{\partial\dot{x}_0}=c\omega+\int_{-d}^{0}C_d\frac{\rho D}{2}\left[\omega\sqrt{(u-\omega\dot{x})^2+w^2}+\frac{\omega(u-\omega\dot{x})^2}{\sqrt{(u-\omega\dot{x})^2+w^2}}\right]dz$$

and

$$\frac{\partial F}{\partial x_0} = k_s$$

Representing x_0 by a Fourier series:

$$x_0 = a_0 + \sum_{n=1}^{N} (a_n \cos n\tau + b_n \sin n\tau), \quad (6a)$$

then we have

$$\dot{x}_0 = \sum_{n=1}^{N} (-n a_n \sin n\tau + n b_n \cos n\tau), \quad (6b)$$

$$\ddot{x}_0 = \sum_{n=1}^{N} (-n^2 a_n \cos n\tau - n^2 b_n \sin n\tau) \quad (6c)$$

and

$$\Delta x_0 = \Delta a_0 + \sum_{n=1}^{N} (\Delta a_n \cos n\tau + \Delta b_n \sin n\tau). \quad (6d)$$

After substituting Eqs (6a) to (6d) to Eq. (5), we have

$$\frac{\partial F}{\partial x_0}\Delta a_0 + \sum_{n=1}^{N}\left(\frac{\partial F}{\partial x_0}\cos n\tau - \frac{\partial F}{\partial \dot{x}_0} n \sin n\tau - \frac{\partial F}{\partial \ddot{x}_0} n^2 \cos n\tau\right)\Delta a_n + \sum_{n=1}^{N}\left(\frac{\partial F}{\partial x_0}\sin n\tau + \frac{\partial F}{\partial \dot{x}_0} n \cos n\tau - \frac{\partial F}{\partial \ddot{x}_0} n^2 \sin n\tau\right)\Delta b_n = -F(\ddot{x}_0, \dot{x}_0, x_0, \tau). \quad (7)$$

Applying the Galerkin method, i.e., multiplying Eq. (7) in turn by 1, $\cos\tau$, $\cos 2\tau$, ..., $\sin n\tau$, and integrating with respect to τ between the limits of 0 and 2π, a set of $2N+1$ equations for the unknown coefficients Δa_0, Δa_1, Δa_2, ..., Δb_n can be found. Hence, a better solution, $x_0 + \Delta x_0$, is obtained from the initial approximate solution, x_0. The procedure is repeated a number of times until a solution of desired accuracy is obtained.

3 Experimental investigations

3.1 Experimental setup

The experimental runs are conducted in the wave flume equipped with the DHI active absorption wave generating system in The Hong Kong Polytechnic University. The physical dimensions of the flume are 25 m long, 1.5 m wide and 1.5 m deep. The experiment set-up is shown schematically in Fig.1a.

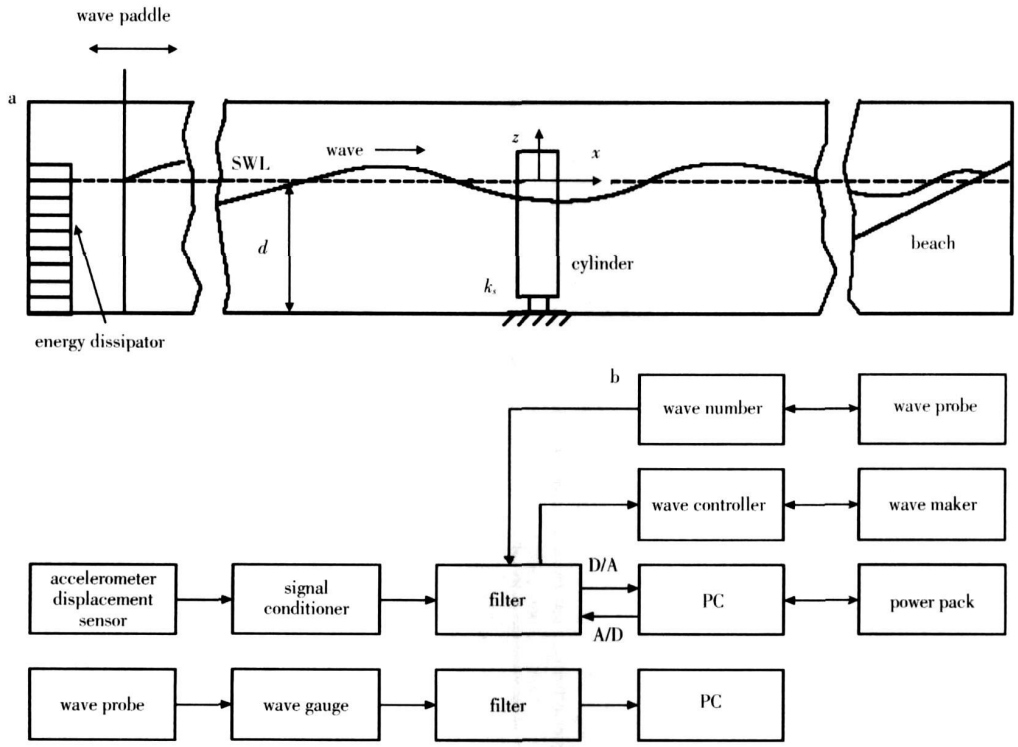

Fig.1. Details of the experimental set-up. a. Vertical cylinder in wave flume and b. measurement of oscillations.

In studying vibration of the vertical cylinders, both the displacements of the cylinders and their accelerations are measured. The schematic diagram of the data acquisition system is shown in Fig. 1b.

Ten capacitance wave gages are used during experimental runs to record the free surface oscillations around vertical cylinders. The principle of the wave gauges is that the capacitance changes with the wetted length of the measuring wire during the passage of wave trains.

3.2 Measurement of structural damping of cylinder system, effective spring stiffness, drag coefficient and intertia coefficient

The cylinders used in the study of the in-line response are made from a plastic tube with an outside diameter of 215 mm and a length of 1×10^3 mm (from No. 1 cylinder to No. 3 cylinder) and 700 mm (No. 4 cylinder). Each cylinder is positioned vertically with its bottom at a distance 600 mm below the water surface by two steel plates having a cross-section of 30 mm×2 mm at its bottom. The accelerometer is located on the top of each cylinder. The mass of each cylinder is about 15 kg. The details are shown in Figs. 2 and 3. For these experiments, No. 1 cylinder to No. 3 cylinder were installed as moving case and No. 4 cylinder as fixed one. The first cylinder was about 5.5 m from the piston-type wave paddle. The basic parameters are shown in Table 1.

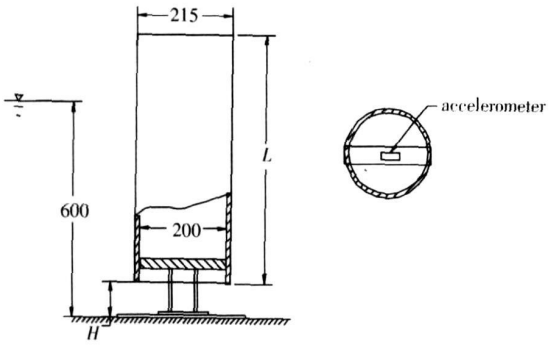

Fig. 2. Sketch of moving cylinder.

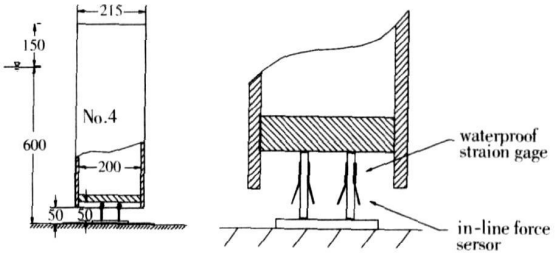

Fig. 3. Sketch of fixed cylinder and the wave force measurement (No. 4 cylinder).

Table 1. Detailed parameters of each cylinder

	No. 1	No. 2	No. 3	No. 4
L/mm	999	994	997	700
H/mm	128	128	132	50
m/kg	14.9	14.7	15.1	N/A
Frequency in air/Hz	2.16	2.16	2.16	N/A
Frequency in water/Hz	1.50	1.62	1.66	N/A

The structural damping and spring stiffness are first determined by allowing the cylinder to oscillate freely in air. The time history of the free oscillation of No. 2 cylinder is shown in Fig. 4. From this time history, it is found that the spring stiffness equals 2.748 kN/m and the structural damping 74 N·s/m. The drag coefficient is then determined by allowing the cylinder to oscillate freely in still water. The time history of one such oscillation is shown in Fig. 5. It is found that the natural frequency of the cylinder is 1.62 Hz and the cylinder mass plus the added mass equals 26.36 kg. The drag coefficient then is obtained from the following expression:

$$C_d=\frac{3T_d\left(\frac{A_0}{A'}-e^{\frac{T_d}{T_d^c}\delta_M}\right)}{8\rho DLA_0\left(e^{\frac{T_d}{T_d^c}\delta_M}-1\right)}=2.26 \qquad (8)$$

where A_0 is the initial displacement of cylinder (i.e., at $t=0$); A' is the displacement of cylinder at $t=T_d/2$, in which T_d is the period of oscillation in still water. The derivation of Eq. (8) is given by Li et al. (1997).

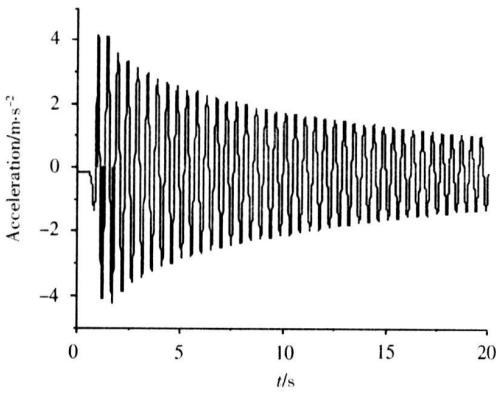

Fig. 4. A record of free vibration of No. 2 cylinder in air.

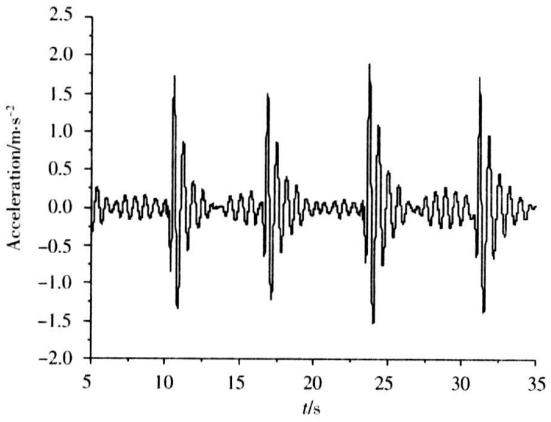

Fig. 5. A record of free vibration of No. 2 cylinder in water.

The inertia coefficient was then determined by measuring the in-line force F_x on the fixed cylinder (No. 4) due to regular waves. Strain gauges are used to measure the strain in the load cell element induced by the wave force. The sensors are a pair of stainless steel plates which have a linear stress-strain characteristics in their elastic range. The stainless steel plates for the in-line force sensors are shorter and thicker than those for displacement sensors to provide the necessary stiffness. For this experiment, bonded strain gauges with waterproofing property are used. The strain gauges are glued directly to the underwater sensors. Four gauges are used for each cylinder. The gauges become the electrical arms of a Wheatstone bridge. The strain of the load cell is proportional to the wave force. Upon proper calibration, the load cell then gives an instantaneous measure of the magnitude of the force generated by the wave. One of the cylinders used in measuring wave force is shown in Fig. 3 and a record of the measurement is shown in Fig. 6. The following expression based on the Fourier averaging technology over one cycle is used for the calculation of the inertia coefficient.

$$C_M = -\frac{\frac{2}{T}\int_0^T F_x \sin\omega t\,dt}{\rho\frac{\pi D^2}{4}L\frac{gH}{2}k\frac{\cosh k(d+z)}{\cosh kd}} = 2.5. \quad (9)$$

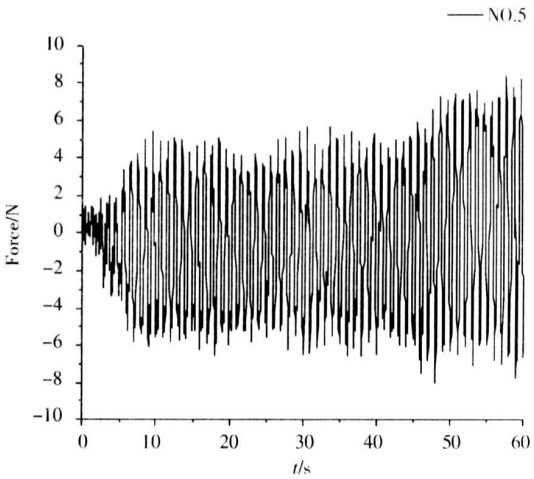

Fig. 6. A record of the measured force in regular waves.

3.3 Response of cylinders in regular and random waves

Both the computed and experimental results for the amplitudes A_1 ($= \sqrt{a_1^2 + b_1^2}$) of the response of a single cylinder at excitation frequency in regular waves at a wave height of 0.01 m are shown in Fig. 7.

The vibration of cylinders and movement of fluid around cylinders have also been investigated in random waves using the JONSWAP spectrum.

In each run, both accelerations and wave height data were recorded at a sampling frequency of 20 Hz for a total of 3 600 data points per channel. In order to investigate the interaction between wave and flexible cylinders, the peak period of JONSWAP spectra was

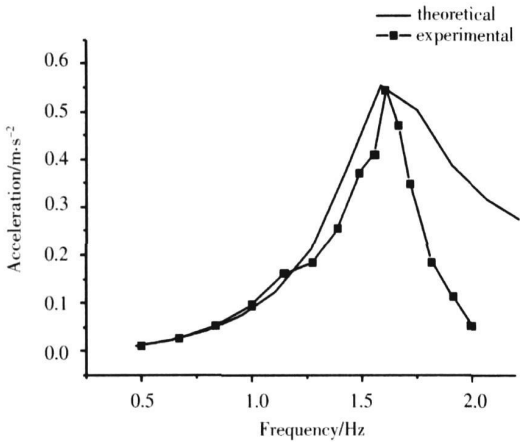

Fig. 7. Comparison between theory and experiment.

set at 2.0 Hz, the value of H_{ms} was 10 mm, and the value of γ was 3.3. The analysis of the collected data was carried out using a standard FFT package. In order to reduce the statistical error in spectral computations, each record containing 3 600 data points was divided into eight parts, each part containing 1 024 points. Neighboring parts have an overlap of 75% of their data points (768 points). In this process certain data points were discarded from either end of each record. Averaging in the frequency domain was done by merging eight consecutive spectral density estimates.

3.3.1. Three vibrating cylinders

The locations of the three cylinders and the ten wave gauges are shown in Fig. 8. Figure 9 shows the power spectra for the response of the three cylinders. The energy transfer between waves and cylinders are shown in Fig. 10 where the spatial variations of wave height amplitude spectra at different locations are plotted. It is important to note that there are two peaks in the spectra of No. 1 cylinder. The first peak of 1.46 Hz is close to the natural frequency of No. 1 cylinder. The second peak of 1.66 Hz is near the natural frequencies of No. 2 cylinder and No. 3 cylinder. It can be seen that the main peaks of No. 2 cylinder and No. 3 cylinder are 1.66 Hz. There is an obvious peak at 1.4 Hz for Gages 15, 16, 17 and 18 and at 1.6 Hz for Gages 15, 16 and 17. The wave height become smaller at Gages 11, 12 and 13. The cylinders absorb some of the wave energy and vibrate at a range of frequencies, but still predominantly near the natural frequencies. Because of the energy transfer to the cylinders, the wave heights behind cylinders are reduced.

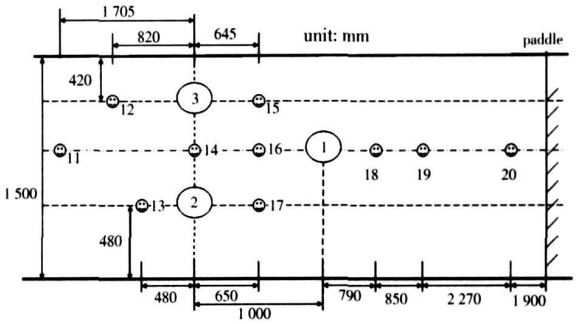

Fig. 8. Sketch of three cylinders.

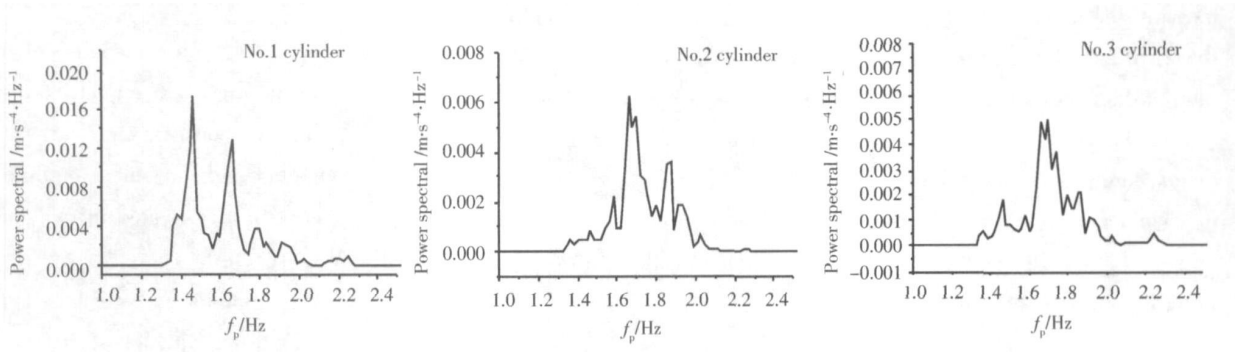

Fig. 9. Response of cylinders in random waves (f_p=2 Hz).

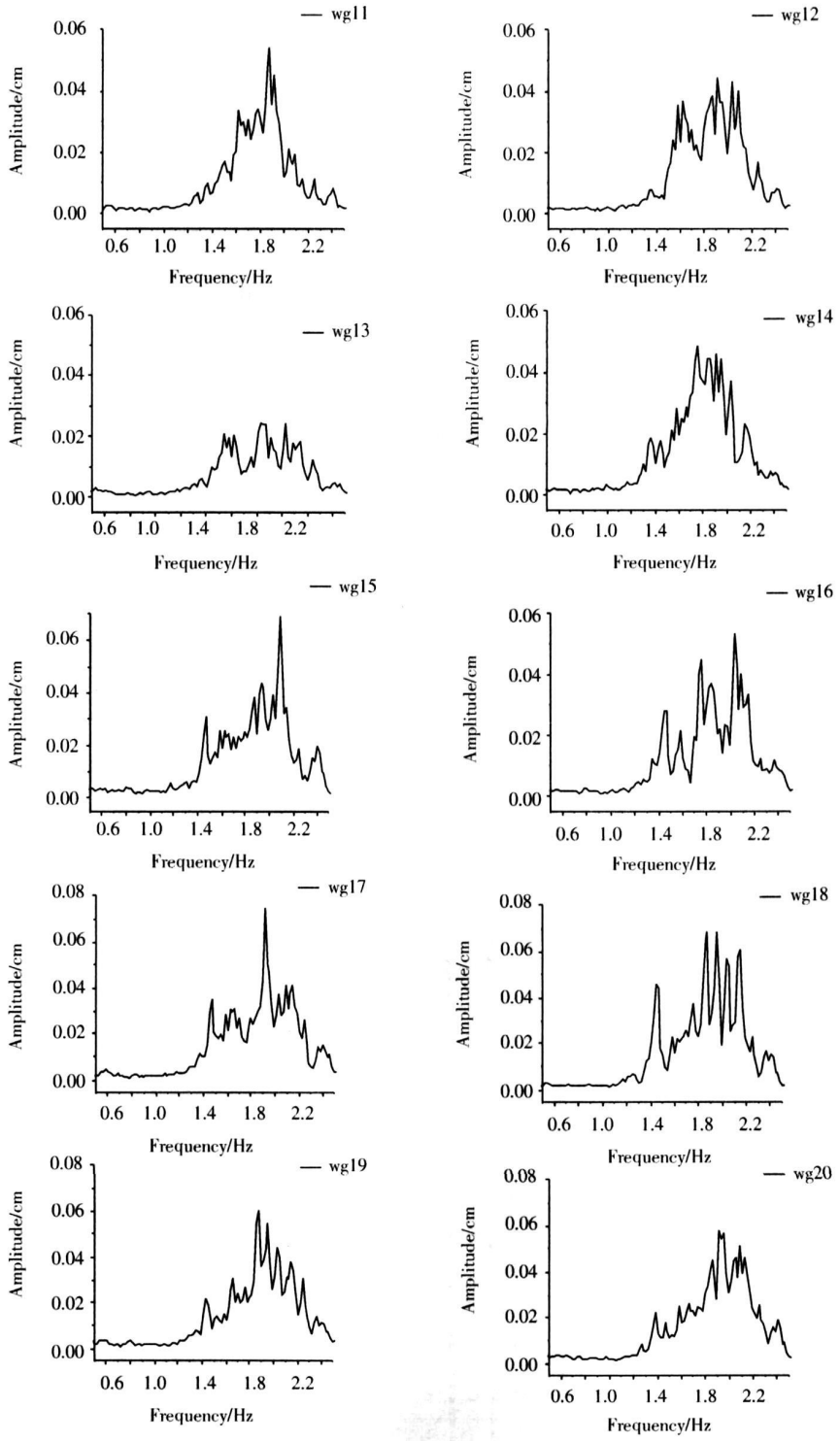

Fig. 10. Spectral evolutions.

When waves travel to the cylinders, a flow of energy begins at the natural frequencies of the cylinders. Finally equilibrium is reached with the result that both the vibrating cylinder spectra and wave height spectra have peak values in the resonance frequencies.

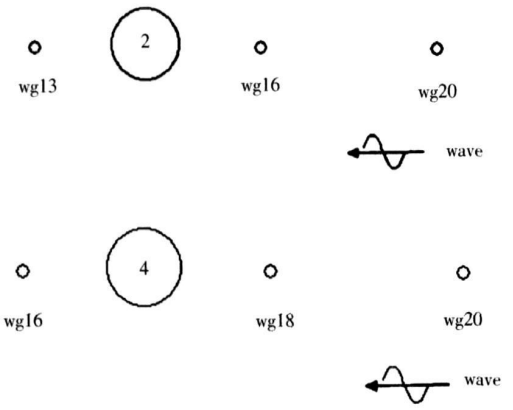

Fig. 11. Sketch of locations of wave gauges. a. Sketch of vibrating cylinder case and b. Sketch of fixed cylinder case.

3.3.2 Wave height analysis for fixed and vibrating cylinders

In order to distinguish the individual effects of wave-vibrating cylinder interactions, it was essential to perform tests for both the vibrating cylinder (No. 2 cylinder) and the fixed one (No. 4 cylinder). For this purpose two different wave frequencies were selected, 1 and 2 Hz. The method of analysis of the collected data was the same as discussed above.

Figures 12 and 13 show the wave spectra around the vibrating cylinder and fixed cylinder, respectively. For the peak frequency with 2 Hz, there is an obvious peak at 1.4 Hz at Gage 13 behind the vibrating cylinder, but this phenomenon has not been observed for the fixed cylinder. It implies that for the peak frequency with 2 Hz there exists a transfer of energy from high frequencies because of the vibration of the cylinder. But for the peak freguency with 1 Hz, only relatively smaller amplitude values are found.

3.3.3 Vibration analysis of single cylinder

It is known that when the ratio of the wave height to the cylinder diameter is small, the nonlinear effects

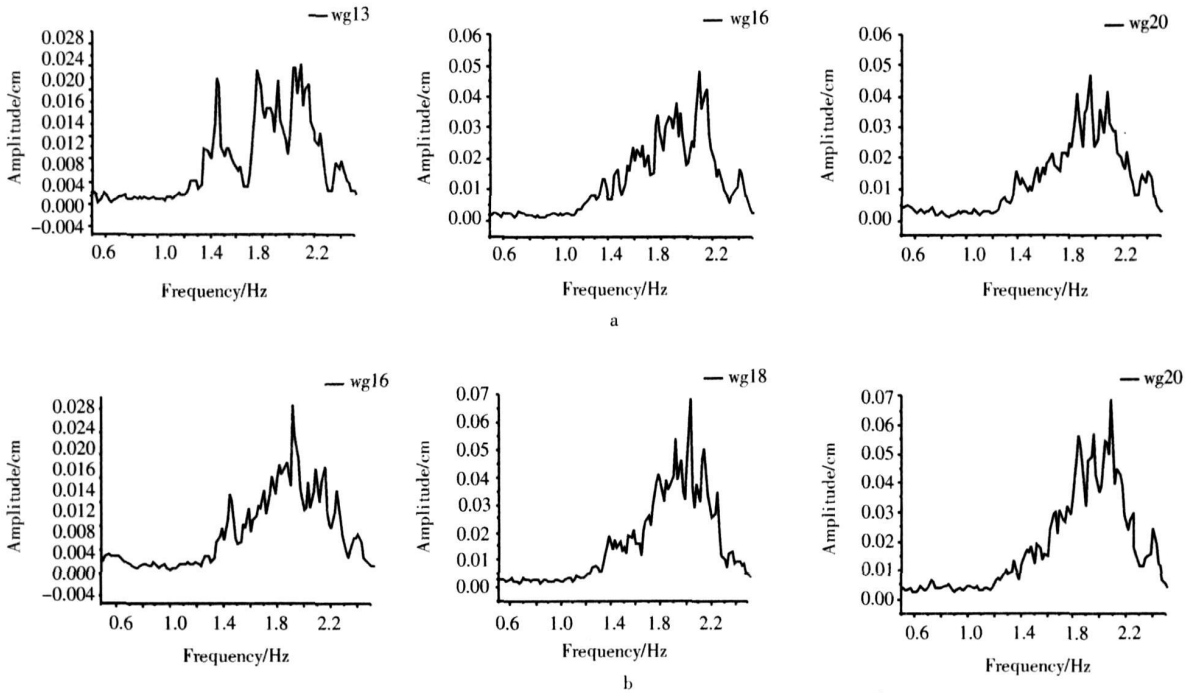

Fig. 12. Comparisons of wave spectra around vibrating and fixed cylinders (f=2 Hz). a. Wave spectra around vibrating cylinder and b. wave spectra around fixed cylinder.

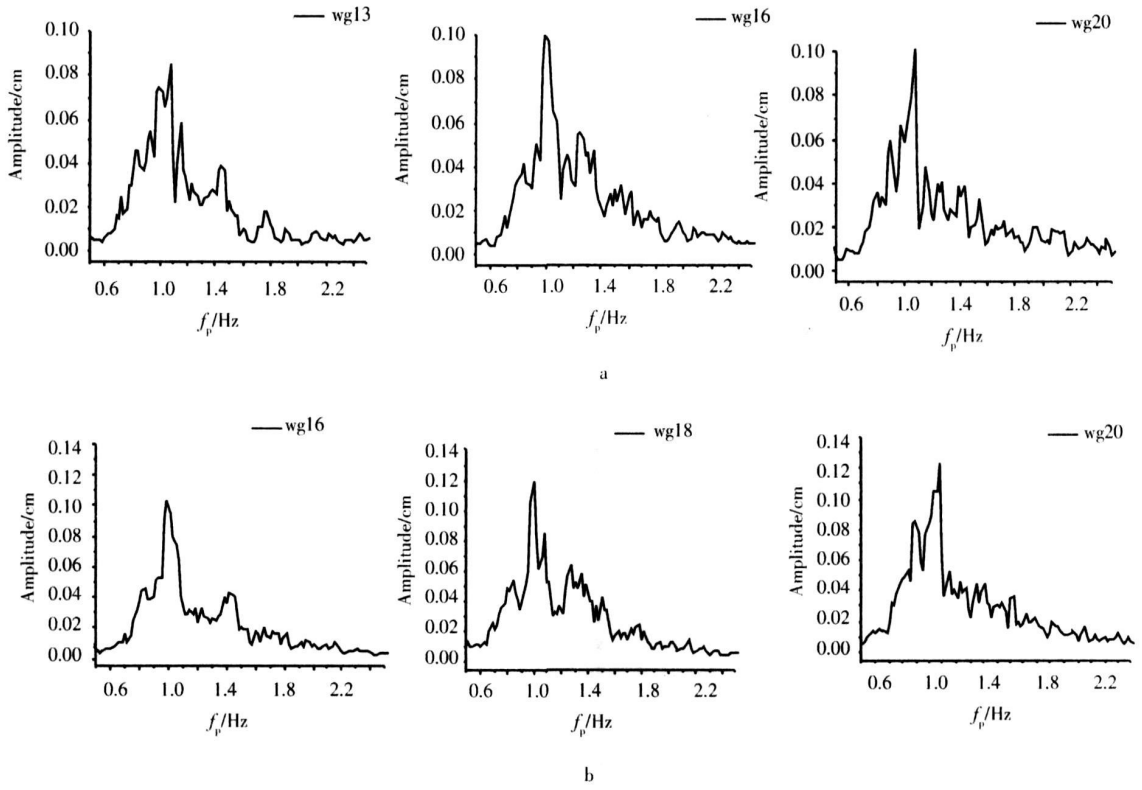

Fig. 13. Comparisons of wave spectra around vibrating and fixed cylinders (f_p=1 Hz). a. Wave spectra around vibrating cylinder and b. wave spectra around fixed cylinder.

are weak and the response of the cylinder to random wave excitation can simply be obtained by superposing the contributions from individual wave components, as described below.

First the surface elevation η, is expressed as

$$\eta = \sum_{i=1}^{n} \frac{H_i}{2} \cos(k_i x - \omega_i t + \phi_i). \quad (10)$$

The amplitudes of the first harmonic A_{1i} of the dynamic response corresponding to each wave component can either be calculated by solving Eq. (7) using the IHB method or obtained from the frequency-response curve. The spectrum of the dynamic response of the cylinder is then given by

$$G_x(f) = \frac{A_{1i}^2}{2\Delta f} \quad (11)$$

where Δf is the chosen frequency-band size.

It can be seen from Figs.14, 15 and 16 that the calculated spectra based on superposition of individual wave components agrees well with the measured spectra, except when the peak frequency equals 1 Hz.

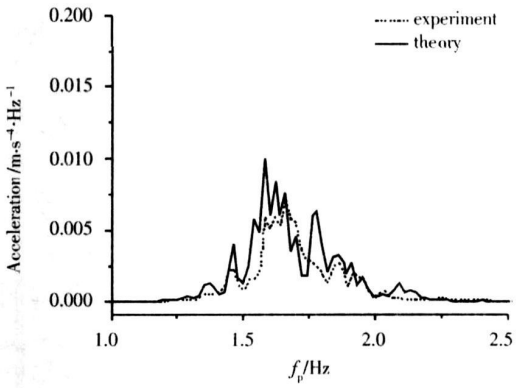

Fig. 14. Theoretical and experimental vibration spectra at the peak frequency with 2 Hz.

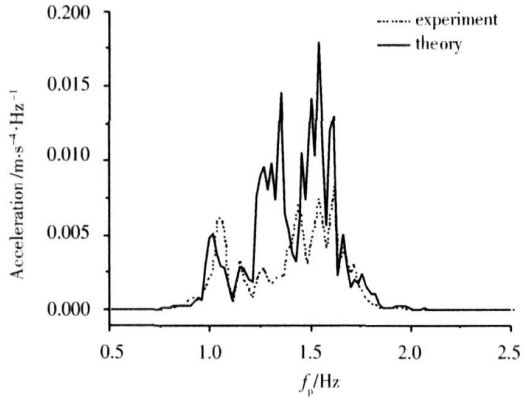

Fig. 15. Theoretical and experimental vibration spectra at the peak frequency with 1 Hz.

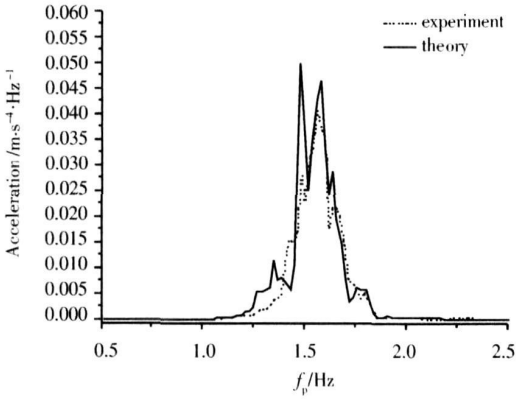

Fig. 16. Theoretical and experimental vibration spectra at the peak frequency with 1.62 Hz.

3.3.4 Vibration analysis of two cylinders position cases

Further experiments were performed to explore the possibility of using superposition of the responses to different wave components to predict the responses of two cylinders as shown in Fig. 17 in random waves. From Fig. 8 to Fig. 23, it is seen that the calculated and measured spectra match well for No. 1 cylinder, but do not fit well for No. 2 cylinder. It is because the wave height used to predict the response of No. 2 cylinder is measured by wave gauge 17, where the direction of wave propagation does not align with the vibration trajectory of No. 2 cylinder because of the presence of No. 1 cylinder. So the calculated peak is higher than the corresponding measured peak.

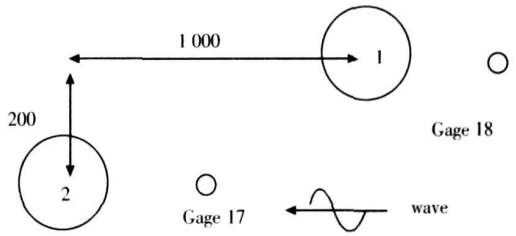

Fig. 17. Sketch of locations of wave gauges.

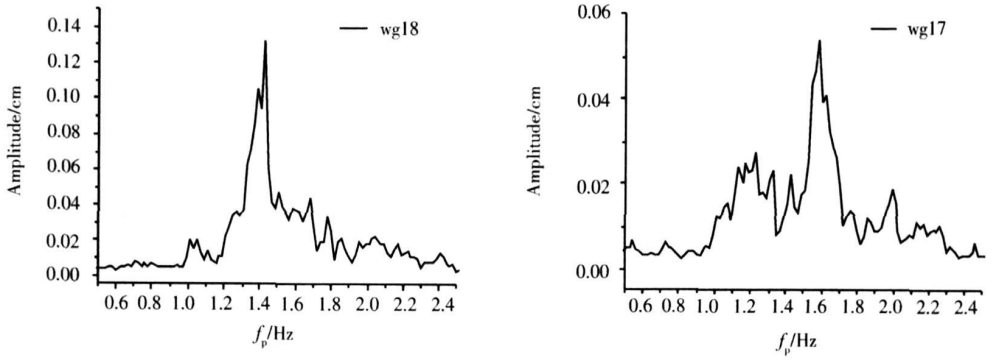

Fig. 18. Wave spectra of Gages 18 and 17 (f_p=1.56 Hz).

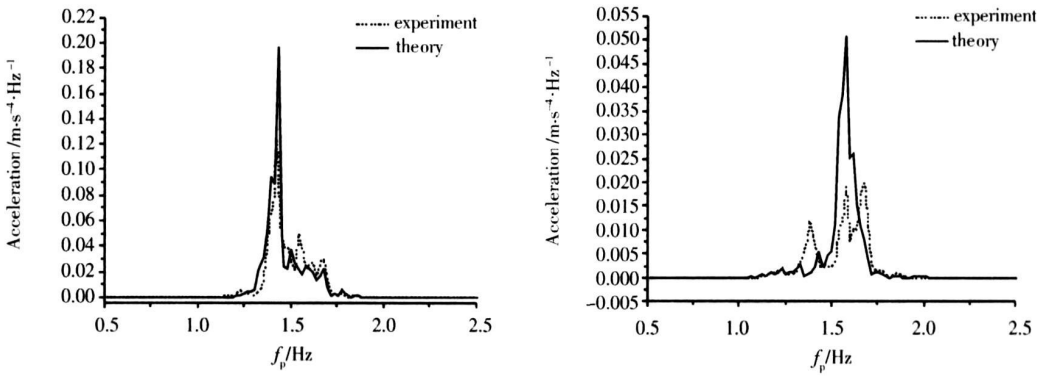

Fig. 19. Theoretical and experimental vibration spectra of cylinders 1 & 2 (f_p=1.56 Hz).

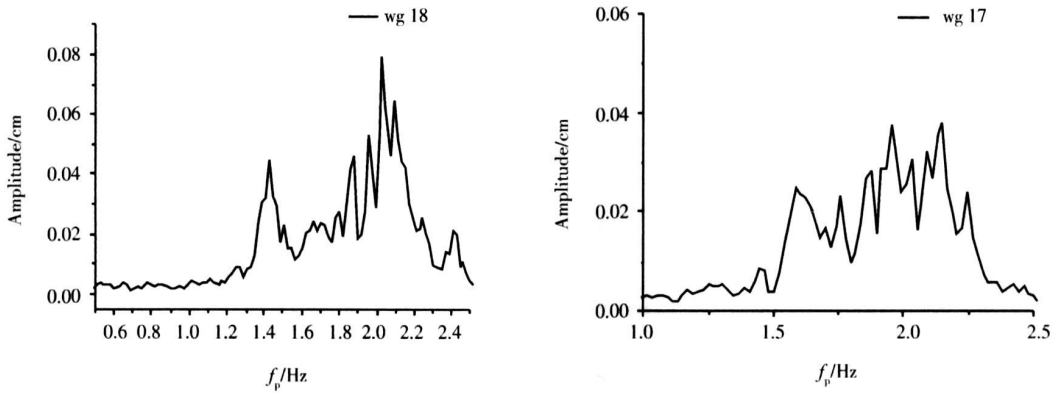

Fig. 20. Wave spectra of gages 18 and 17 (f_p=2 Hz).

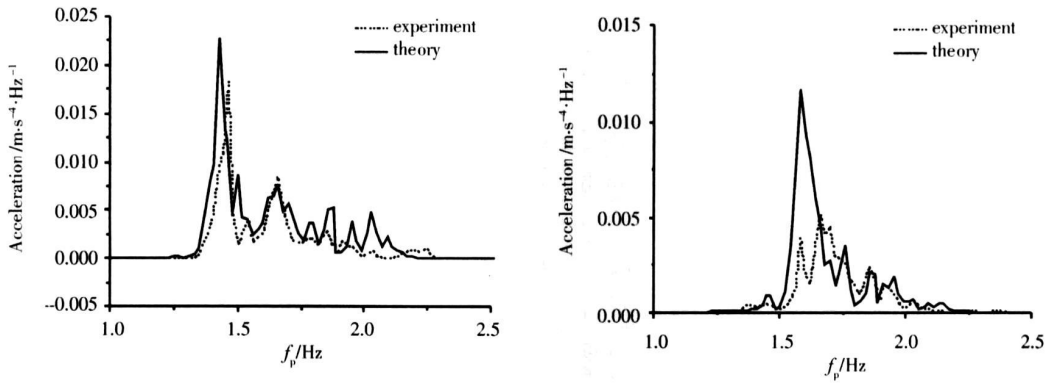

Fig. 21. Theoretical and experimental vibration spectra of the cylinders 1 and 2 (f_p=2 Hz).

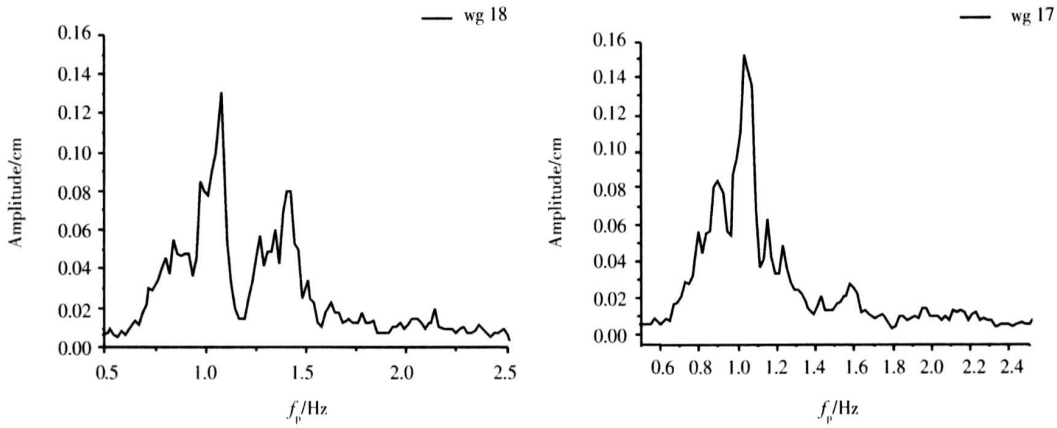

Fig. 22 Wave spectra of Gages 18 and 17 (f_p=1 Hz).

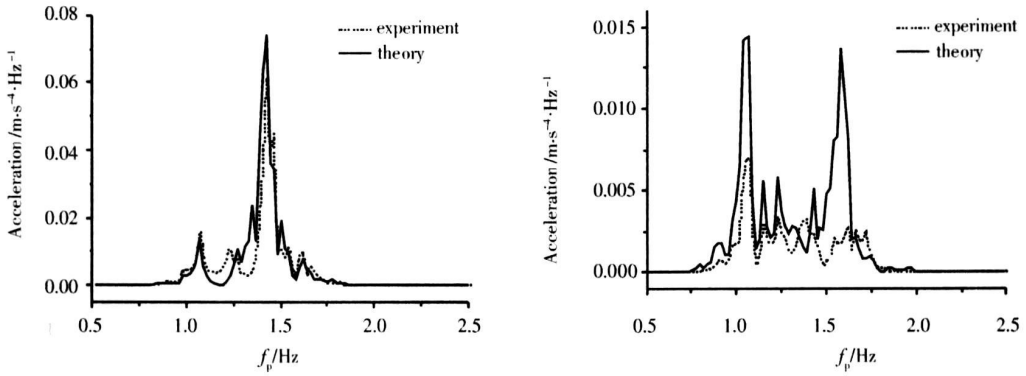

Fig. 23 Theoretical and experimental vibration spectra of the cylinders 1 and 2 (f_p=1 Hz).

3.3.5 Wave attenuation analysis

The wave attenuation performance of a vertical flexible cylinder was compared with that of a fixed one. Regular waves of different periods (i.e., T=0.5, 1, 2 s) were used. The wave heights in front of and behind the cylinder were measured. Figure 12 shows the results of these two cases. The parameters was used to assess the attenuation characteristic of the cylinder, where $\bar{s}$ is the mean square value of the wave height defined by

$$\bar{s}=\frac{1}{T}\int_0^T \eta^2(t)\,dt$$

The attenuation coefficient, Ac, is defined as

$$Ac=\left(1-\frac{\bar{s}_{re}}{\bar{s}_{fr}}\right)\times 100\%.$$

where subscripts fr and re mean front and rear.

Table 2 The attenuation coefficient of vibrating cylinder

T_p/s	m_{fr}/mm^2·s	m_{re}/mm^2·s	Ac(%)
0.5	0.106	0.053	50
1	0.226	0.149	34
2	0.102	0.110	−8

Table 3 The attenuation coefficient of fixed cylinder

T_p/s	m_{fr}/mm^2·s	m_{re}/mm^2·s	Ac(%)
0.5	0.096	0.066	31
1	0.186	0.1626	13
2	0.146	0.1998	−37

It was observed that the vibrating cylinder was superior to the fixed one in reducing the wave height. The coefficient of wave attenuation due to regular waves for a vibrating cylinder ranges from —8% to 50% and for the fixed one from —37% to 31%. It was found that the waves of high frequencies can be more readily attenuated than low frequency ones. This aspect is now under further investigation and will be reported in a future paper.

4 Conclusions

The present study confirms that the Morison equation for predicting the in-line response of a flexibly mounted vertical cylinder in regular waves do not agree well with the experimental results when the ratio of wave length to cylinder diameter is larger than 0.35. The theoretical predictions of the cylinder response obtained by solving the Morison equation using the incremental harmonic balance method agree well with experimental measurement provided the above limiting ratio is not exceeded. The vibration of cylinders and movement of fluid around cylinders have also been investigated in random waves using the JONSWAP spectrum. The cylinders absorb the energy near their natural frequency bands. This causes a transfer of energy, beginning at the neighboring frequencies of the natural frequencies of the cylinders. The in-line response in random waves can be predicted using the experimental frequency-response curve by a superposition of the responses to different wave components only when the ratio of wave height to cylinder diameter is small. This study will be useful to the design of energy dissipating type vertical cylinders, such as flexible breakwaters for wave attenuation.

Acknowledgements

The work was supported by the National Natural Science Foundation of China under contract No. 10272118 and The Hong Kong Polytechnic University Research of China under contract No. A—PE28.

References

Angrilli F, Cossalter V. 1982. Transverse oscillations of a vertical pile in waves. Journal of Fluids Engineering, 104: 46~53

Broderick L L, Leonard J W. 1995. Non-linear response of membranes to ocean waves using boundary and finite-elements. Ocean Engineering, 22 (7): 731~745

Chaplin J R, Rainey R C T, Yemm R W. 1997. Ringing of a vertical cylinder in waves. Journal of Fluid Mechanics, 350: 119~147

Chen B F. 1998. Hybrid three-dimensional finite-difference and finite-element analysis of seismic wave induced fluid-structure interaction of a vertical cylinder. Ocean Engineering, 25 (8): 639~656

Chern M J, Borthwick A G L, Taylor R E. 2001. Simulation of non-linear free surface motions in a cylindrical domain using a Chebyshev—Fourier spectral collocation method. International Journal for Numerical Methods in Fluids, 36 (4): 465~496

Hayashi K, Chaplin J R. 1998. Vortex-excited vibration of a vertical circular cylinder in waves. International Journal of Offshore and Polar Engineering, 8: 66~73

Kaye D, Maull D J. 1993. The response of a vertical cylinder in waves. Journal of Fluids and Structures, 7: 867~896

Lau S L, Cheung Y K. 1981. Amplitude incremental variational principle for non-linear vibration for elastic system. Journal of Applied Mechanics, 48: 959~964

Lau S L, Zhang W S. 1992. Non-linear vibrations of piecewise-linear systems by incremental harmonic balance method. Journal of Applied Mechanics, 59: 153~160

Li Y S, Zhan S, Lau S L L. 1997. In-line response of a horizontal cylinder in regular and random waves. Journal of Fluids and Structures, 11: 73~87

McIver P, McIver M, Zhang J. 2003. Excitation of trapped water waves by the forced motion of structures. Journal of Fluid Mechanics, 494: 141~162

Miu Guoping, Liu Yingzhong. 1991. Wave and hydrodynamic forces on multiple large vertical cylinders of arbitrary sec-

tion. Acta Oceanologica Sinica (in Chinese), 13 (5): 729~735

Murata K, Takahashi K, Kato Y, 2004. Underwater shock and bubble pulse loading against model steel cylinder. Explosion, Shock Wave and Hypervelocity Phenomena in Materials. Materials Science Forum, 465~466: 283~287

Qiu Dahong, Zhu Datong, 1985. Calculation of wave forces acting on cylinder group. Acta Oceanologica Sinica (in Chinese), 7 (1): 86~102

Qiu Dahong, Zhu Datong, 1986. Wave force on pier group. Acta Oceanologica Sinica, 5 (2): 301~312

Sarkar A, Taylor R E, 1998. Low-frequency responses of non-linearly moored vessels in random waves: development of a two-scale perturbation method. Applied Ocean Research, 20 (4): 225~236

Sarkar A, Taylor R E, 2001. Low-frequency responses of nonlinearly moored vessels in random waves: coupled surge, pitch and heave motions. Journal of Fluids and Structures, 15 (1): 133~150

Sarpkaya T, Isaacson M, 1981. Mechanics of Wave Forces on Offshore Structures. New York: Van Nostrand Reinhold

Sawaragi T, Nakamura T, Miki H, 1977. Dynamic behavior of a circular pile due to eddy shedding in waves. Coastal Engineering in Japan, 20: 109~120

Swan C, Taylor P H, van Langen H, 1997. Observations of wave-structure interaction for a multi-legged concrete platform. Applied Ocean Research, 19 (5~6): 309~327

Tatsuno M, Bearman P W, 1990. A visual study of the flow around an oscillation circular cylinder at low Keulegan—Carpenter numbers and low stokes numbers. Journal of Fluid Mechanics, 211: 157~182

Williamson C H K, 1985. In—line response of a cylinder in oscillatory flow. Applied Ocean Research, 7: 97~106